Miniaturization and Performance Enhancement of Super Wide Band Four Element MIMO Antenna using DNG Metamaterial for THz Applications

Ranjana Kumari (ranjana.biet@gmail.com)
Galgotias College of Engineering and Technology
V. K. Tomar
GLA University
Ankit Sharma
Galgotias College of Engineering and Technology

Research Article

Keywords: Super wide band, THz application, Four-port MIMO antenna, Envelope correlation coefficient (ECC), Channel capacity loss (CCL), SRR-CC unit cell.

Posted Date: March 14th, 2022

DOI: https://doi.org/10.21203/rs.3.rs-1430251/v1

Miniaturization and Performance Enhancement of Super Wide Band Four Element MIMO Antenna using DNG Metamaterial for THz Applications

Ranjana Kumari[1,2], V. K. Tomar[1], Ankit Sharma[2]

[1]Department of Electronics & Communication, GLA University, Mathura, Uttar Pradesh, India
[2]Galgotias College of Engineering and Technology, Greater Noida, Uttar Pradesh, India

Email:ranjana.biet@gmail.com, vinay.tomar@gla.ac.in, ankit.deli@gmail.com

Abstract

A compact semi-hexagonal-shaped MIMO antenna loaded with a planar SRR (split-ring resonator) structure is presented for Terahertz applications. The single radiating element consists of a semi-hexagonal shape metallic patch loaded with SRR-CC (Split ring Resonator-Connected C shape) metamaterial unit cell to enhance the impedance bandwidth as well as gain of the proposed antenna. The proposed antenna element can be easily extended into two-port and four-port MIMO antenna configurations. Four radiating elements of the proposed antenna are printed on 122.4*122.4 um^2 quartz substrate having a thickness of 10 um. The radiating elements are placed orthogonally to achieve high isolation and miniaturization in the MIMO system. The proposed antenna exhibits super-wide impedance bandwidth ($S_{11}\leq$ -10dB) in the range of 0.9–10.1 THz (with fractional bandwidth of 168% at f_0=5.5 THz) while isolation of antenna is more than 20 dB in the whole operating band. The peak gain of the antenna is 7.51dBi with more than 95% radiation efficiency in the entire band. The stable radiation pattern, high gain, high radiation efficiency, and good diversity performance of the proposed antenna make it suitable for many THz applications such as breast cancer detection, sugar measurement, drug detection.

KEYWORDS: *Super wide band ,THz application. Four-port MIMO antenna, Envelope correlation coefficient (ECC), Channel capacity loss (CCL), SRR-CC unit cell.*

1. Introduction

Because of high spectral efficiency, wide bandwidth, high penetration power, and low interference noise Terahertz spectrum have attracted a lot of researchers' interests to design application based antennas in Jamshed et al.(2020).Nowadays, researchers have focused to design antennas for terahertz applications such as biomedical imaging(Zhang et al.2021), cancer detection(Thakur et al.(2021)),material characterization(Koenig et al.(2013), THz sensing(Vafapour et al.(2020), space and earth applications (Maagt 2007). Further, to utilize the THz regime because of simple features and low manufacturing cost, various planar microstrip geometries-based antennas are designed in Ushaben et al.(2021);H. Davoudabadifarahani et al.(2019) for different applications.However, planar microstrip antennas have low bandwidth and low radius of radiation. To enhance the performance of microstrip antenna, photonic crystal is utilised as substate in R. K et al.(2018) . However, this antenna suffers from high radiation losses in THz regime .The researchers in Kumud et al.(2010), a microstrip patch antenna has been designed for dual-band operation.However, its

size is not compact and resonates at only dual frequencies for surveillance system and not able to cover multiple applications. Therefore, it is necessary to design an ultra-wide band (UWB) antenna to cover many applications.Therefore, In Singhal(2019a;b) have utilized elliptical shape in a single element to achieve wideband and high gain for THz spectrum. However, it has been observed that the gain, as well as radiation efficiency, are very poor at lower THz frequencies. In the literature review, many researchers(Ushaben et al. 2021; H. Davoudabadifarahani et al.2019; R. K et al. 2018; Kumud et al. 2010; and Singhal 2019a;b)have focussed only on designing single element antenna for THz regime . However, to enhance the channel capacity of the THz system, MIMO antennas are employed. Author in King (2014) explains the usages of MIMO antennas which helps to increase data rate, channel capacity without increasing the antenna's transmitting power and spectrum resources in the THz communication system .

To acquire these demands, many researchers (Varshney et al. 2019; Luo et al. 2019; Babu et al. 2022; Okan 2021; Saxena and Awasthi 2020;and Singhal 2020 a;b;c) have been focused to design MIMO antenna systems for THz applications. To ensure the functioning of MIMO communication system, self-interference between radiating elements must be minimum. Therefore, a graphene-based MIMO antenna with pattern diversity has been designed in Varshney et al.(2019) for narrow THz spectrum (1.76 THz to 1.87 THz) with good mutual coupling between elements . In Luo et al.(2019), a graphene tunable FSS structure has been implemented between radiating elements to achieve high isolation for narrow THz frequency spectrum. In (Babu et al. 2022; Okan 2021), mutual coupling between two radiating elements has been achieved by employing spatial and pattern diversity techniques. Apart from this, numerous two-port MIMO antenna systems with wide spectrum for SWB operation have been designed in (Saxena and Awasthi 2020;and Singhal 2020 a;b;c). A super wideband MIMO antenna has been designed with impedance bandwidth (0.33-10THz) for high-speed THz applications in Saxena and Awasthi (2020). However, the designed antenna is not compact with low gain as well as radiation efficiency at sub-THz frequencies as compared to higher THz frequencies. A spatial diversity-based MIMO antenna is discussed in Singhal (2020 a) having isolation of more than 23 dB and the footprint of antenna configuration is printed on polyimide substrate having size 820*1000*81.29 μm^3. In (Singhal 2020 b;c) , tetradecagonal ring and windmill shapes are utilized to design the MIMO antenna for super wideband operation. Furthermore, many existing two-port MIMO antennas have been reported for super wideband (SWB) operation and also observed to have low peak gain(dBi) and radiation efficiency(%) in sub-THz frequency range as compared to higher frequency spectrum.

Therefore, in this article, planar SRR-CC metamaterial loaded semi hexagonal MIMO antenna is proposed to enhance gain as well as impedance bandwidth, and minimize self-interference among radiating elements. The key contributions of the proposed antenna are (1) compact size of 0.37 λ *0.37 λ *.03 λ; (2) fractional impedance bandwidth of 168%; (3) number of ports are four with good isolation; 4) overall low profile with high efficiency and omnidirectional patterns with maximum peak gain 7.51 dBi.This paper is divided into different sections. Evolution steps of the single radiating element with analysis of SRR-CC unit cell, formation of two and four-port MIMO antenna and equivalent diagram of proposed four port MIMO antenna are discussed in Section 2. Results & discussions of the proposed antenna are discussed in Section 3. In Section 4, the conclusions of the proposed antenna are drawn.

2. Designing of Proposed MIMO antenna

The proposed antenna is designed on a 10 um thick quartz substrate with dielectric constant (Ɛr) 3.75 and tangent loss of 0. 0001. Quartz substrate has been characterized by low loss factor over a wide frequency spectrum in (Davies et al.2018 and Miao Z.W et al.2019) . The design of a four-port MIMO antenna is divided into three sub-sections.

a. Evolution of SRR-CC unit cell loaded Single element

Fig.1 elucidates the evolution stages of single radiating element with SRR-CC. The evolution procedure is divided into four stages. In stage 1, a simple microstrip feed line rectangular patch with partial ground is designed on substrate with dimensions 61x61.3x10 μm^3 as shown in Fig 1(a). According to simulated results (S11) as in Fig2, stage 1 patch antenna offers dual resonance having the -10 dB impedance bandwidth 1.25 to 2.2THz and 4.7 to 5.8 THz, respectively. To achieve wide bandwidth, two triangular shape slots have been etched out from the lower edge of radiating element with the partial ground as depicted in Fig 1(b). The -10 dB impedance bandwidth is 1.2 to 4.8 THz as illustrated in Fig 2. The fractional bandwidth is improved by 65% but the objective of the designed antenna is to achieve 0.9 to 10 THz. Further, to enhance impedance bandwidth, an offset semi-circular slot is etched out from the upper edge of radiating element as depicted in stage 3. As shown in the simulated results, the impedance band has been achieved from 1.8 to 7.9 THz with fractional bandwidth of 126 % at 4.85 THz.

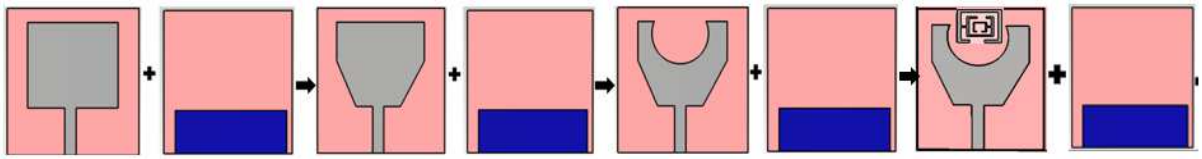

(a) Stage 1 (b) Stage 2 (c) Stage 3 (d) Stage 4 (Final)

Fig 1. Evolution stages of single radiating element

To further enhance fractional bandwidth as well as gain(dBi) in the intended spectrum, an SRR-CC is implanted on the upper edge of radiating element in stage 4 (final stage). Comparison of stage1- stage4 is done by s-parameters of the single radiating element as illustrated in Fig 2. Finally, construction of single element configuration is designed in stage-4 having fractional bandwidth 168 % at operating frequency 5.5 THz. Simulated results of single-element antenna containing SRR -CC structure show that fractional bandwidth of stage 4 is 48% wider than stage 3.It is clear from Fig. 2 that SRR based metamaterial (MTM) unit improves the overall impedance bandwidth of the antenna specifically in the lower band. Further, SRR-CC also helps in improving isolation between the radiating elements. Authors in (Ali et al.(2019);He et al.(2011) , metamaterial with negative (permittivity, permeability, and refractive index) characteristics are designed to enhance the antenna's bandwidth, efficiency, and gain. Therefore, to improve the impedance bandwidth and isolation of antenna, Pan et al.(2016) has been designed a DNG (Double negative) MTM. According authors in Balmaz et al.(2002), SRR is a common MTM that is artificially produced to generate anticipated magnetic field in various metasurface.

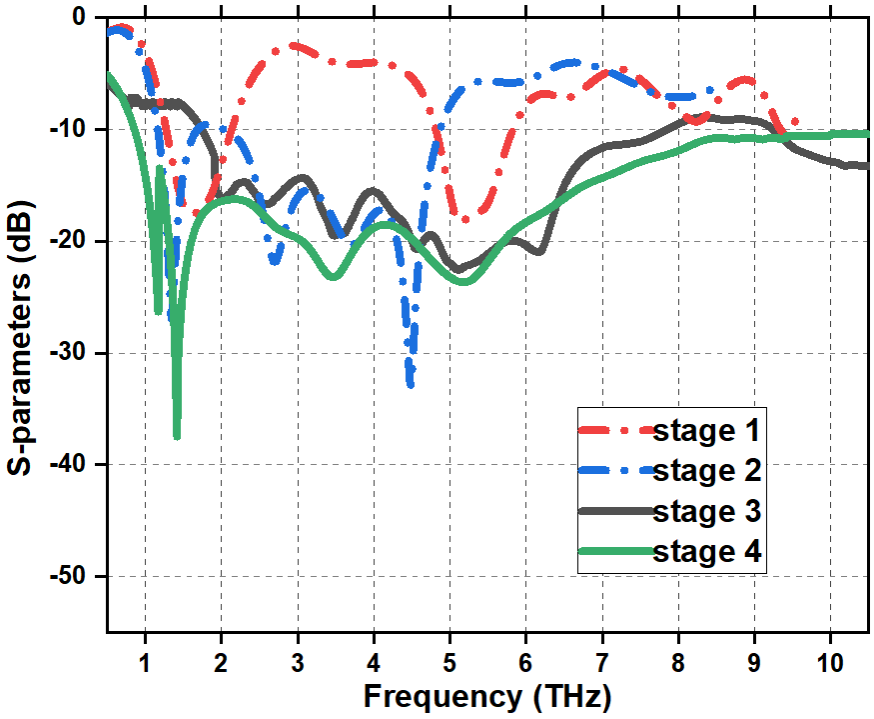

Fig 2. Simulated S-parameters of evolution stages (single element)

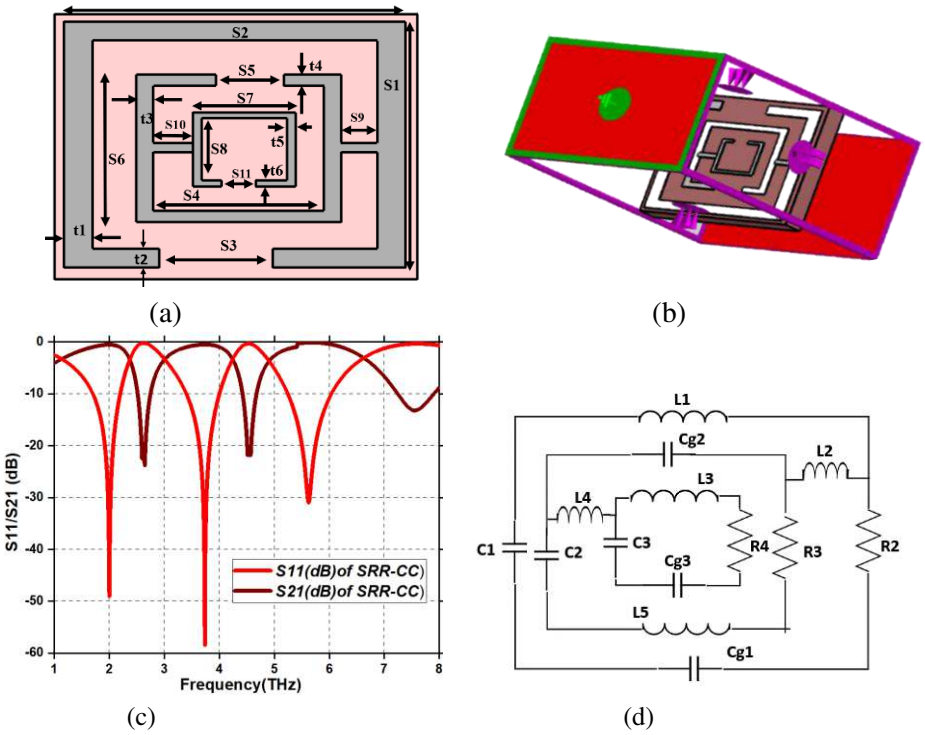

Fig 3. (a)-(d) Geometric layout, boundary conditions arrangement of planar SRR-CC unit cell, and S11 and S21 of unit cell, equivalent circuit

Authors in Tung et al.(2009) has been analyzed that Negative refractive index in planar structure could be attained when permittivity is negative.To produce triple-band resonance with negative (permittivity, permeability, and refractive index) in intended spectrum (0.9-10.1THz), three opposite concentric metallic rectangle rings are printed on the top latyer of quartz

substrate which creates magnetic resonance on excitation and produce a vertical magnetic field. This vertical magnetic field retains negative permittivity values with respect to frequency. The split gaps among metallic rings produce capacitances that are effecient to control the resonace of planar structure. The optimized physical dimensions of SRR-CC unit cell has been illustrated in fig.3(a) and physical dimentions are shown in table 1.To evaluate the effective parameters of unit cell to understand the working mechanism, a finite integration techniques (FIT) based on electromagnetic simulation CST microwave studio has been used. A SRR-CC unit cell has been placed between two ports of positive Z-axis and negative Z-axis. To energize the unit cell electromagnetic wave is applied towards Z axis. The perfect electric (PE) and perfect magnetic (PM) boundary conditions are applied along the x-axis and y-axis as illustrated in fig3(b).After simulation, analysis of SRR-CC is done by scattering parameters as illustrated in Fig3(c).Simulated unitcell is resonanting at three resonant frequencies 2THz, 3.6 THz and 5.6THz to cover intended spectrum 0.9 to10.1THz and also exhibits the broad range of negative (permittivity, permeability, and refractive index) as illustrated in fig 4(a)- fig 4(c).

To validate the simulated results of the SRR-CC, the Nicolson-Ross-Wier (NRW) approach has been utilized to compute the permittivity, permeability, refractive index.This approach initially calculate v_1 & v_2 from addition and substraion of S11(dB) and S21(dB)in Smith et al.(2002).The computation of permittivity, permeability, refractive index is done by following the equation (1)-(5).

$$\mu_r = \frac{2}{jk_0\, t} \times \frac{1 - v_2}{1 + v_1} \tag{1}$$

$$\epsilon_r = \frac{2}{jk_0\, t} \times \frac{1 - v_2}{1 + v_1} \tag{2}$$

$$\eta_r = \frac{2}{jk_0\, t} \sqrt{\frac{(S_{22} - 1)^2 - {S_{22}}^2}{(S_{22} + 1)^2 - S_{22}^2}} \tag{3}$$

In equation (1)-(3), t is thickness of substrate, k_0 is wave number, $v_1$and v_2 are scattering parameters. Scattering parameters have been calculated as following equations

$$v_1 = S_{21} + S_{11} \tag{4}$$

$$v_2 = S_{21} - S_{11} \tag{5}$$

The effective permittivity(ϵ_r), effective permeability (μ_r), and refractive index (η_r)of a SRR unit cell are illustrated in Fig 4(a) -Fig4(c).The frequency range of permittivity, permeability , refractive index, and the double negative region has been shown in table (2).The double negative regions are 2.0-3.0 THz, 3.9-4.4 THz, 5.3-6.4THz, and 7.3-7.5 THz respectively. The double negative regions(DNG) exhibit that a unit cell can be utilized for sensing and detecting THz applications in Smith et al.(2002). To investigate the original place of such low absorption in that frequency regime, the electric field is inspected at 5.5THz. Fig.4(d) shows that the right half of the resonator has a large concentration of electric field. This field is connecting three rings which intensify the total electric field and exhibit high reflection and low absorption at a particular frequency. This produces magnetic field resonance along electric field resonance which is needed to raise absorption levels. According to geometric layout of SRR-CC, a split gap of the ring resonator produces the capacitance which help to control resonance and metal

loop of ring produce inductance its value introduce the vertical magnetic field. The vertical magnetics field employ the negative permittivity values. The equivalent diagram of SRR-CC is illustrated in Fig.3(d).The equivalent capacitance of split gaps and inductance of metal loops are calculated by equation (6)-(7).

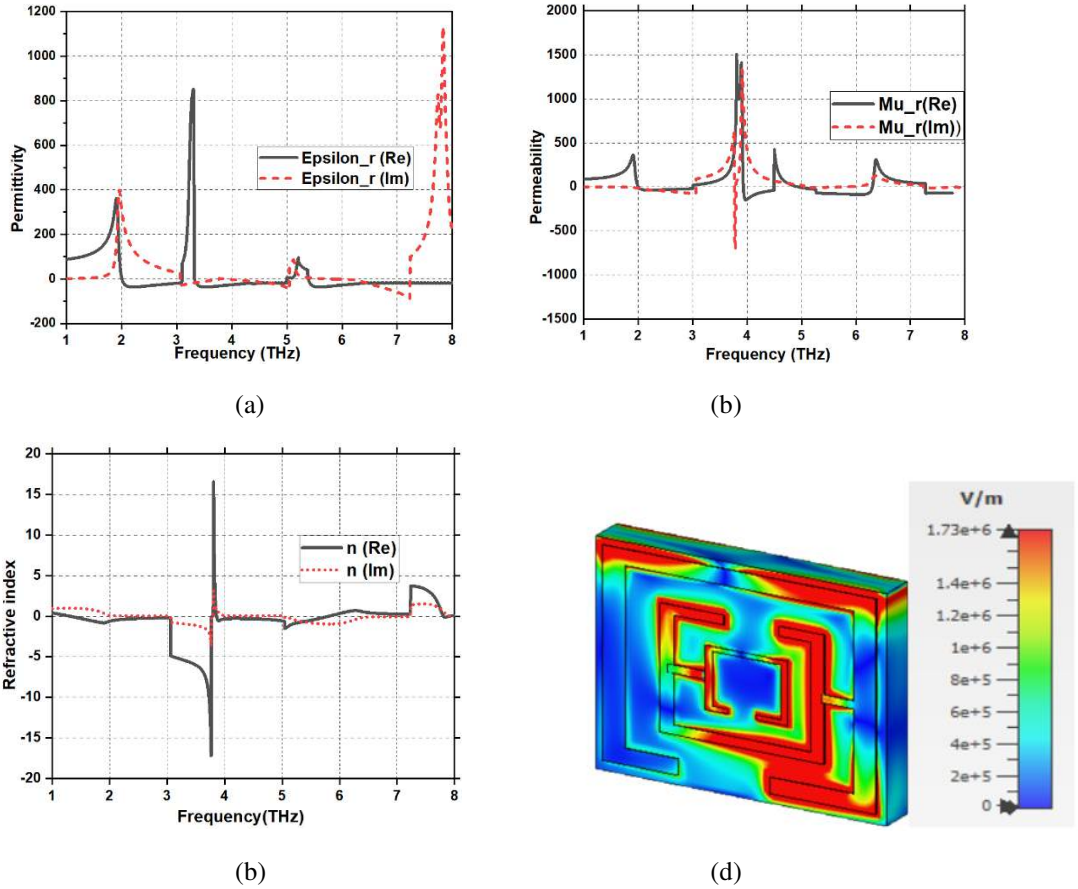

Fig 4.(a)-(d) permittivity, permeability, and refractive index respectively and Electric field distribution at 5.5THz.

Table 1. Unit cell dimensions

Parameters	Dimensions (μm)	Parameters	Dimensions (μm)
S1	13	**S2**	18
S3	10	**S6**	7.8
S4	9	**S5**	3.6
S8	3.3	**S7**	5.4
S11	1.8	**S9**	1.9
S10	2	**t1**	1.5
t2	1	**t3**	1
t4	0.6	**t5**	0.4
t6	0.3	**t**	10

Table 2. Negative effective parameters vs frequency region of a unit cell

Parameters	Frequency region of Negative index in THz
Effective permittivity	2.0 - 3.2, 3.4 - 5.0, 5.3 - 7.5
Effective permeability	2.0 - 3.0 ,3.9 - 4.4, 5.0-6.4, 7.3-7.5
Effective refractive Index	1.5-3.45, 4.0 - 5.5
Effective Double Negative Region (DNG)	**2.0 - 3.0, 3.9-4.4, 5.3-6.4, 7.3-7.5**

b. Formation of diversity based two-port MIMO antenna

In this section, the optimized single-element antenna has been transformed into a two-port MIMO antenna, and further, two-port antenna has also been investigated utilizing spatial and pattern diversity techniques. The optimized spatial diversity-based two-element MIMO antenna is illustrated in Fig. 5(a). The geometric dimensions of two element of MIMO antenna are given in table 3. The simulated result of S-parameters of this configuration is shown in Fig. 5(b) with wide impedance bandwidth of 0.9 to 10.1 THz. The impact of SRR-CC on isolation between radiating elements is illustrated in fig 5(b). In MIMO system, isolation among radiating elements should be less than -15db and due to the closeness of radiating elements, isolation (S12/S21) of the proposed antenna without SRR-CC is poor in frequency range from 1.0 to 1.7 THz as well as 7 to7.7 THz as illustrated in Fig 5 (b). Further improve the isolation in these frequency ranges, SRR-CC is implanted on top of radiating elements. According to simulated results, the mutual coupling between two elements has been improved in frequency range 3.0 THz to 10.1THz. Isolation is highest at 8.3THz and at 2.5THz, isolation is acquired 16dB which is acceptable range only. Therefore, furthermore enhance the isolation two-ports between radiating elements, a pattern diversity-based MIMO antenna is designed.

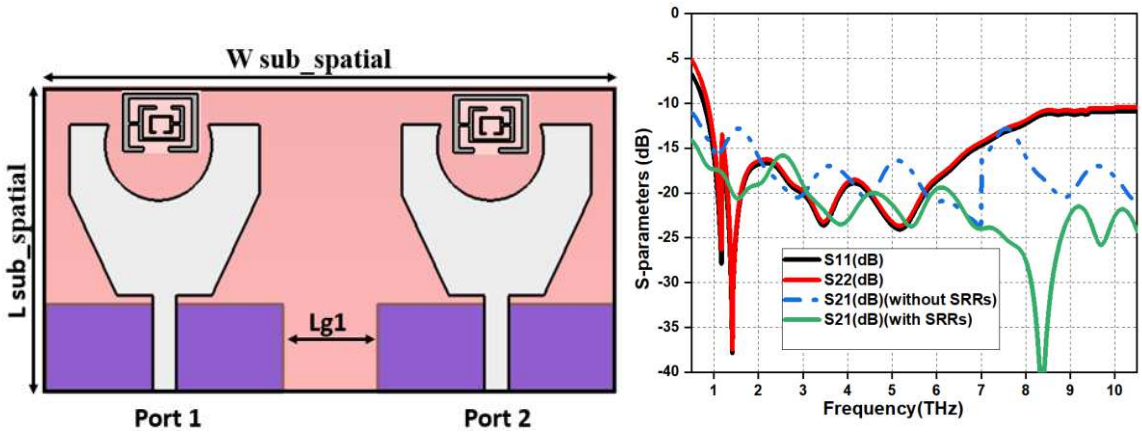

(a) (b)

Fig 5. (a)Two port MIMO antenna with spatial diversity (b) Simulated results of scattering parameters

A pattern-diversity approach is utilized to design a two-port MIMO antenna. The top and bottom view of the antenna is illustrated in Fig 6a(i)-(ii). The SRR-CC loaded two radiating elements are also placed orthogonally to each other and the minimum allowable space between

elements is L3. According to the illustration of S-parameters in Fig6 (b), the proposed antenna is operating from 0.9 to 10.1THz and the mutual coupling effect between elements is analyzed by transmission coefficient (S21/S12 in dB). It is observed that designed MIMO antenna is offering isolation of more than 25 dB in the intended frequency spectrum. So, the proposed antenna exhibits good diversity performance in the wideband frequency spectrum. Isolation among radiating elements is also explained by surface current density (A/m) in next section.

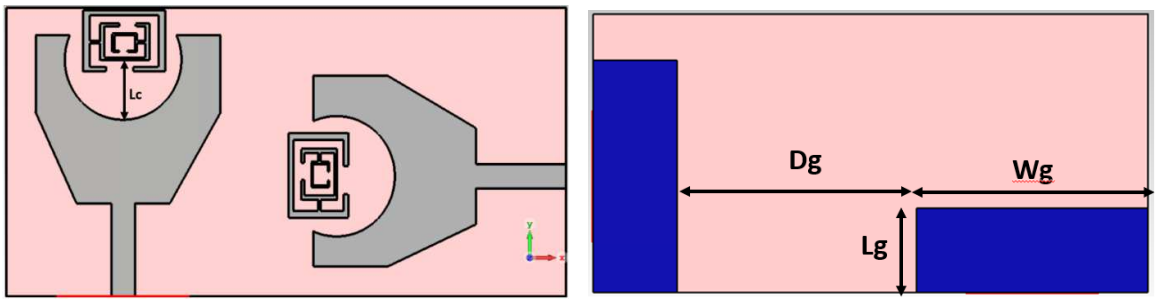

(i) Top view (ii) bottom view

Fig 6(a)(i)- Fig 6(a)(ii) Top and bottom view of two element MIMO antenna with unit cell

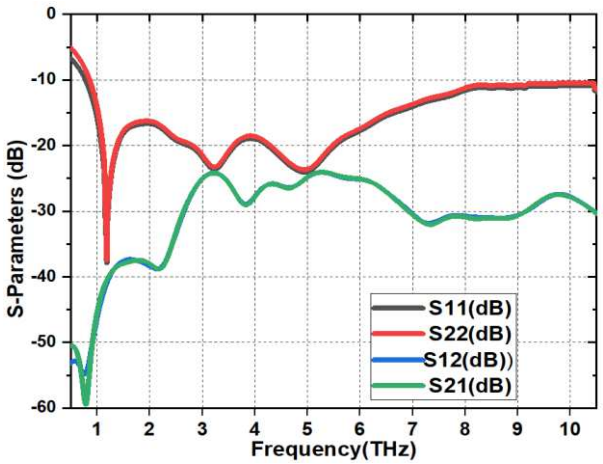

Fig 6(b). Scattering parameters of two-port MIMO antenna with metamaterial

c. Formation of four-port MIMO antenna

Furthermore, to enhance the bandwidth and improvement in isolation among radiating elements, a four-element MIMO antenna is proposed and illustrated in Fig.7(a)-(c). Quartz substrate of dimension 122.4*122.4*10 μm^3 is utilized to print four radiating elements on top of substate as portrayed in Fig 7(a) and ground of radiating elements with four SRR-CC are printed on the backside of substrate as portrayed in Fig7(b). The geometric dimensions of proposed four pot MIMO antenna are given in table 3.An inclined view of the proposed antenna with substrate thickness 't' is depicted in Fig.7(c).The According to Fig 7(c), antenna elements(A1-A4) are placed orthogonally to each other to achieve good isolation. Simulated results of S-parameters are illustrated in Fig. 7(d). As depicted in Fig 7(d), the proposed antenna is operating in the range of 0.9 to 10.1 THz, and transmission coefficients which show the mutual coupling among elements are less than -20 dB in the entire frequency spectrum. These results exhibit good performance in THz communication system.

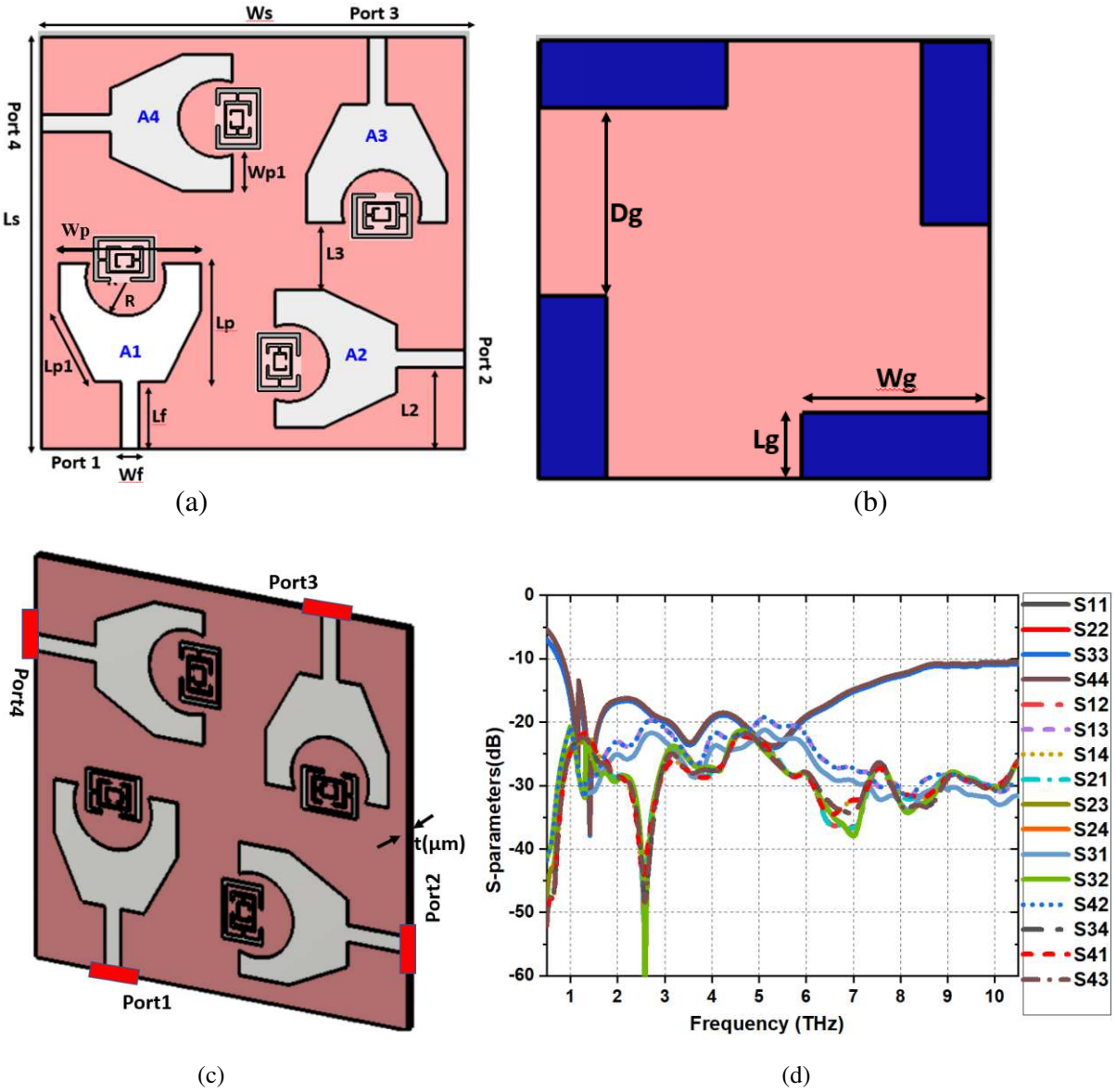

Fig 7. (a)-(c) Front view, back view, and Inclined view of proposed MIMO antenna (d)Simulated S-parameters characteristics of four proposed antenna

d. Equivalent circuit model of proposed Antenna

The equivalent circuit diagram of proposed four-port antenna loaded with SRR-CC is shown in Fig 8. In Cao et al.(2012),each radiating element is represented by a parallel RLC circuit comprising resistance Rp, inductance Lp, and capacitance Cp. Each radiating element is excited by port with 50 ohm resistance. According to authors in Iqbal (2018) and Iqbal (2019) , always some coupling associated with nearby antennas in MIMO system and coupling between antennas is modeled by L_cC_c series lumped components in Fig 8. In the circuit diagram of SRR-CC, split gap of the inner ring is represented by capacitance, and metal loop of ring represented by inductance as shown in Fig3(d). The electric resonance is generated by combination of splits. Magnetic field resonance is generated by the combination of metal loops when electromagnetic signal is applied at both side of planar SRR-CC unit cell structure.The formation of capacitances between split is represented by the following equation (6).

$$C_{split}(fF) = \varepsilon_0 \varepsilon_r \frac{A}{d} \tag{6}$$

In equation (7), ε_0 , ε_r are free space permittivity and relative permittivity, A is area of split and d is distance between split. According to transmission line theory in Cao et al.(2012), inductance can be computed by following equation (8).

$$L_s(pH) = 2X10^5 l \left[\ln\left(\frac{l}{w+t_f}\right) + 1.193 + 0.02235\frac{w+t_f}{l}\right] Cg \tag{7}$$

In equation Cg is correction factor 0.54-0.17, l(length of microstrip feedline), w (width of microstrip line), t_f (thickness of microstrip line).

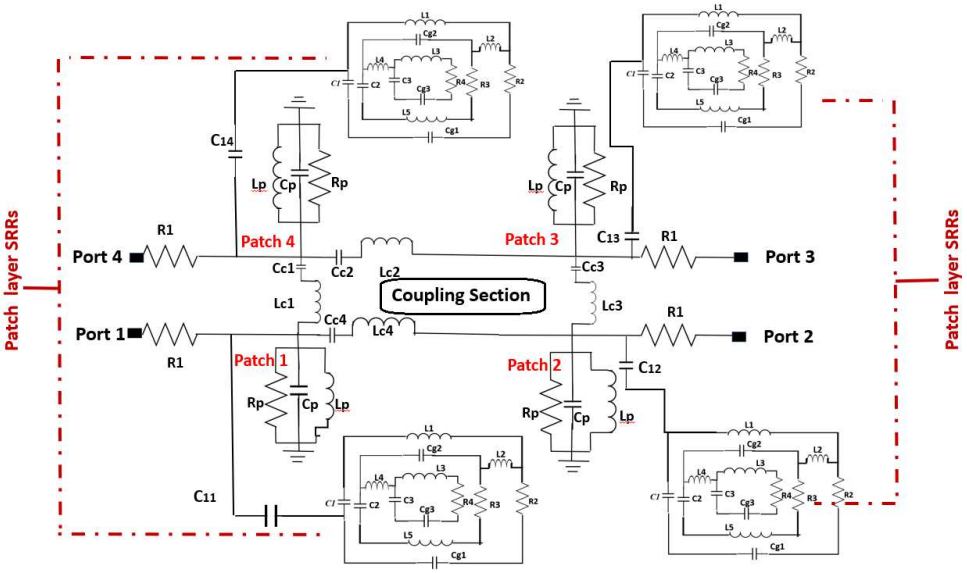

Fig 8. Equivalent Circuit model of four-element MIMO antenna

Table 3. Dimensions of the proposed antenna

Parameters	Dimensions (µm)	Parameters	Dimensions (µm)
Ls	122.4	Wp	40.4
Ws	122.4	Lp	35.6
Wf	5	Lp1	21.2
Lf	19.8	R	14
L2	23	L3	20.3
Dg	52.8	Lg	18.5
Wg	51.3	Wp1	9.6
t	10	L sub_ pattern	61.2
W sub_ pattern	122.4	Lg1	17

3.Result & Discussions

The proposed antenna is designed and simulated using CST Microwave Studio 2019. The simulated results of peak gain (dBi) and efficiency of the proposed antenna are illustrated with and without SRR-CC in Fig 9(a) and Fig 9(b). According to the results, peak gain of proposed antenna with SRR-CC has more than 2 dB gain as compared to the antenna without SRR-CC and proposed antenna shows consistent gain in the entire impedance bandwidth. The total efficiency of four-port MIMO antenna with and without SRRs depends on mutual coupling factor among radiating elements in Thummaluru et al.(2019) . It is calculated by equation (8).

$$Total\ effeciency = radiation\ effeciency * (1 - |S_{11}|^2 - |S_{12}|^2 - |S_{13}|^2 - |S_{14}|^2) \quad (8)$$

The radiation efficiency is more than 95 % and the total efficiency is greater than 80% in THz frequency spectrum of proposed antenna.

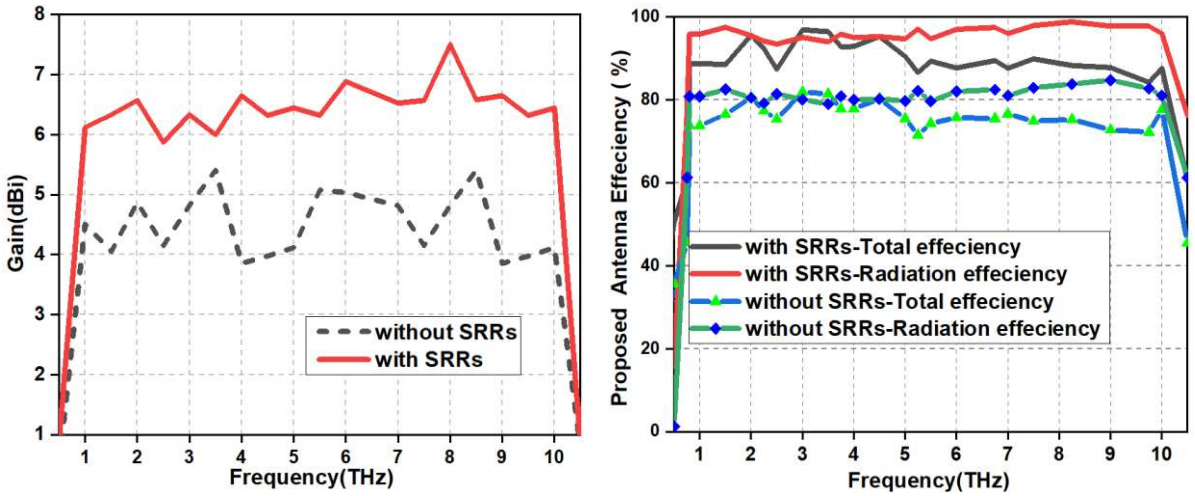

(a) (b)

Fig 9 (a) Simulated result of peak gain (dBi) (b) Simulated results of Total and radiated efficiency

The isolation improvement can easily understand by surface current distribution across radiating elements of the proposed MIMO antenna. The surface current distribution among radiating elements at different frequencies like 2 THz, 6 THz, 8 THz, and 10THz are depicted in Fig 10(a)-Fig 10(d).It is noticed that the maximum amount of surface current (A/m) is concentrated near feed lines and upper edges of radiators when one port is excited and non excited radiating element has minimum amount of surface current distributions(A/m). Therefore, this is evident of isolation among elements. The orthogonal placement of radiating elements with SRRs are utilized to minimize the current density and mutual coupling across antenna elements. Fig 11(a)- Fig 11(c)- illustrates the normalized 2D radiation pattern of the proposed antenna at 2, 8, and 10THz frequencies in XZ plane and YZ plane. To analyse radiation pattern in XZ plane and YZ plane, port 1 of antenna is excited. It is clear, patterns are nearly omnidirectional in both planes as illustrated in Fig 11.

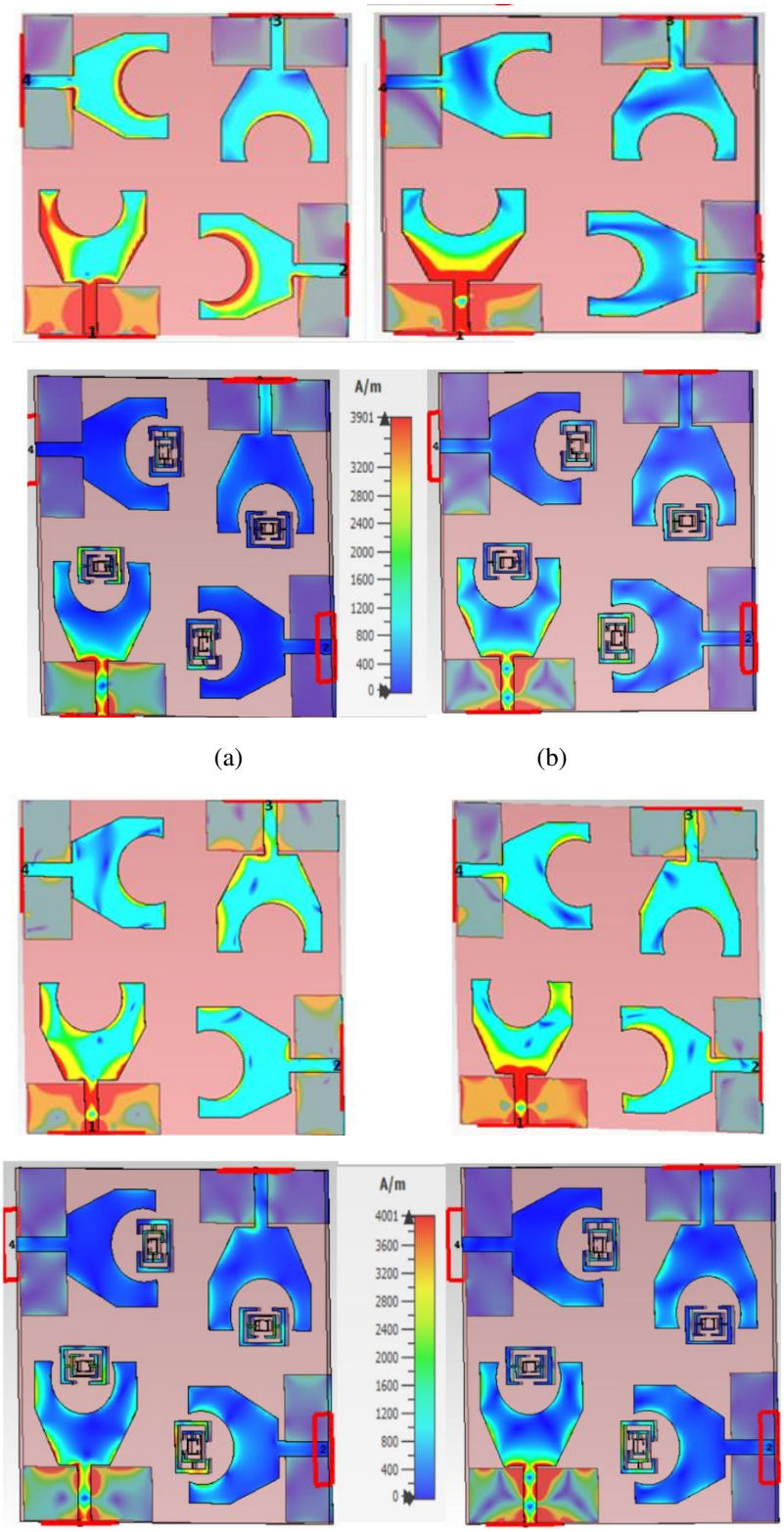

(a) (b)

(c) (d)

Fig 10. Simulated Surface current distribution with and without SRRs at frequency(a) 2 THz (b) 6THz (c) 8THz (d) 10THz

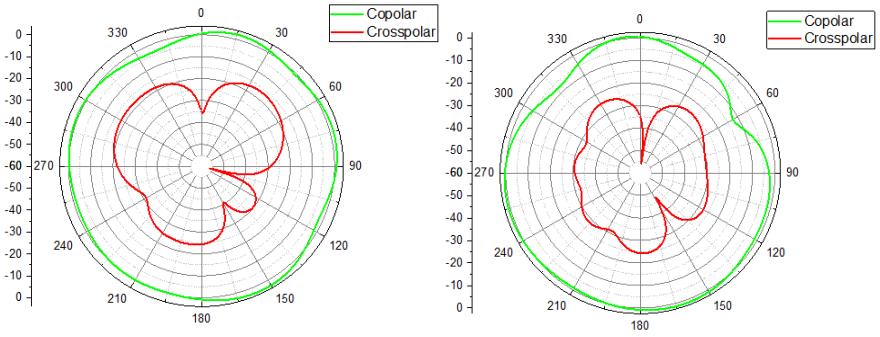

(a)

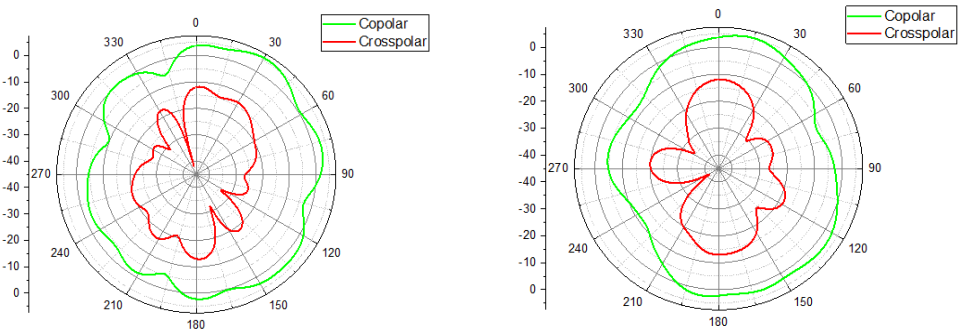

(b)

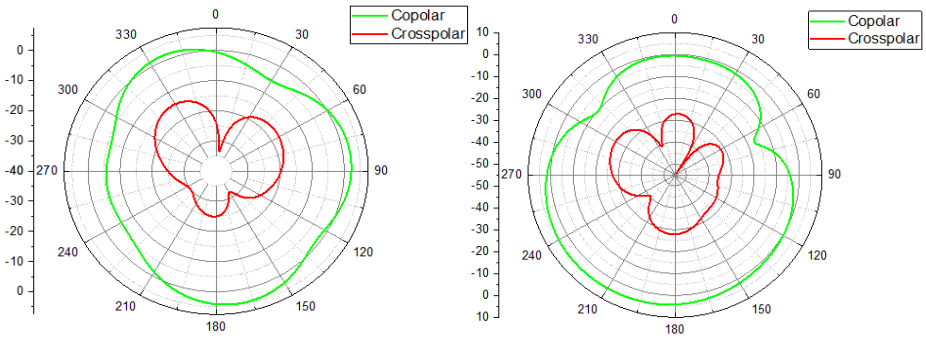

(c)

Fig 11. Simulated radiation patterns of proposed antenna at (a) 2THz (b) 8THz (c) 10THz

a. Diversity Performance Analysis of proposed MIMO antenna

To validate the diversity performance of four port MIMO antenna, few additional parameters are analysed and illustrated in Fig. (12)-Fig. (13). The parameters include envelope corelation coefficient (ECC), diversity gain (DG), multiplexing efficiency "η", total active reflection coefficient (TARC), and channel capacity loss (CCL) and mean effective gain (MEG).

ECC is calculated to measure isolation among radiating elements in wireless communication system in Babu et al. 2022. ECC between i^{th} and j^{th} radiating element can be computed by S-parameters in equation (9).

$$\rho_{ecc,ij} = \frac{\left[\sum_{n=1}^{N} S_{ni}^{*} S_{nj}\right]^2}{\left(1-\sum_{n=1}^{N}|S_{ni}|^2\right)\left(1-\sum_{n=1}^{N}|S_{nj}|^2\right)} \quad (9)$$

To achieve more accurate results, value of ECC is calculated by radiating field of proposed antenna in Saxena and Awasthi(2020). Where XPR is cross-polarization ratio of incident wave in propagation environment. The cross-polarization ratio for outdoor is XPR=1 dB and XPR=6dB for indoor propagation.

$$\rho_{ecc,ij} = \frac{\left|\int_0^{2\pi}\int_0^{\pi}\left(XPR.E_{\theta i}.E_{\theta j}^{*}.P_{\theta}+E_{\varphi i}.E_{\varphi j}^{*}.P_{\varphi}\right)d\Omega\right|^2}{\int_0^{2\pi}\int_0^{\pi}\left(XPR.E_{\theta i}.E_{\theta i}^{*}.P_{\theta}+E_{\varphi i}.E_{\varphi i}^{*}.P_{\varphi}\right)d\Omega X\int_0^{2\pi}\int_0^{\pi}\left(XPR.E_{\theta j}.E_{\theta j}^{*}.P_{\theta}+E_{\varphi j}.E_{\varphi j}^{*}.P_{\varphi}\right)d\Omega} \quad (10)$$

Ideally, ECC value should be zero but practically should be less than 0.5. Therefore, ECC of proposed antenna is calculated by S-parameters and simulated value of ECC in intended spectrum is less than .0025 which exhibits the good diversity performance of proposed MIMO antenna for THz applications as depicted in Fig 12(a). Diversity gain of proposed MIMO antenna is computed by equation (11). In Babu et al. 2022, diversity gain computation depends on ECC value of antenna. To achieve diversity gain near 10db, practically correlation among ports should be less than 0.5. Fig (12)a illustrates simulated results of diversity gain among ports of radiating elements. Simulated value of diversity gain of antenna is 9.99 in entire spectrum which exhibits satisfactory performance of proposed antenna.

$$DG = 10 * \sqrt{1 - ECC^2} \quad (11)$$

Mean effective gain (MEG) is antenna's capability to receive the electromagnetic signals in multipath environment and also elucidated as ratio of received average power at ports to total power received by placing two antennas in same route in Saxena and Awasthi(2020). The acceptable range should be equal or less than to ±3dB in multipath environment. Simulated results of MEGs in gaussian and isotropic medium are illustrated in Fig12(b).To validate the MEG, reported antenna is also simulated in isotropic medium as well as gaussian medium at XPR=0dB and 6dB. Simulated values of MEG are less than -3dB in Gaussian and isotropic medium, which validate the diversity performance of proposed antenna.

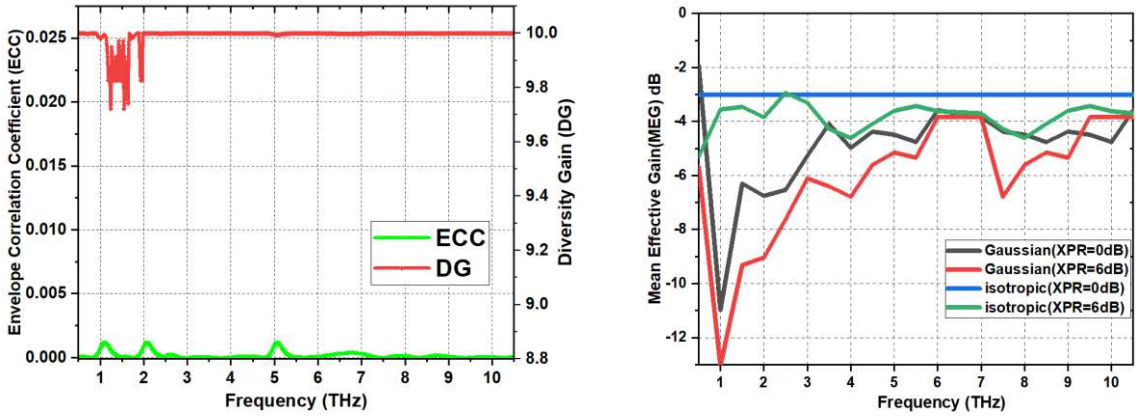

(a) (b)

Fig 12(a)-(b) Simulated results of ECC ,DG and Mean Effective Gain (MEG) in Gaussian & isotropic medium

Channel Capacity Loss (CCL) is another parameter to analyse the performance of MIMO system. The channel capacity grows linearly with number of radiating elements and correlation among radiating elements induce the capacity loss in MIMO system channel.According to Saxena and Awasthi(2020), CCL should be less than 0.4 bit/s/Hz and CCL computation of proposed antenna is done by equation (12)-(15). According to simulated results in Fig13(a), the CCL of proposed MIMO antenna is less than 0.15 bps/Hz in entire spectrum which exhibits satisfactory diversity performance of the proposed antenna in a multipath fading environment.

$$C_{loss} = -\log_2|\varphi^p| \tag{12}$$

$$\varphi^p = \begin{bmatrix} \rho 11 & \rho 12 \\ \rho 21 & \rho 22 \end{bmatrix} \tag{13}$$

$$\rho_{ii} = 1 - \left(|S_{ii}|^2 + |S_{ij}|^2\right) \tag{14}$$

$$\rho_{ij} = (S_{ii}^* S_{ij} + S_{ji}^* S_{ij}) \text{ where i, j= 1or 2} \tag{15}$$

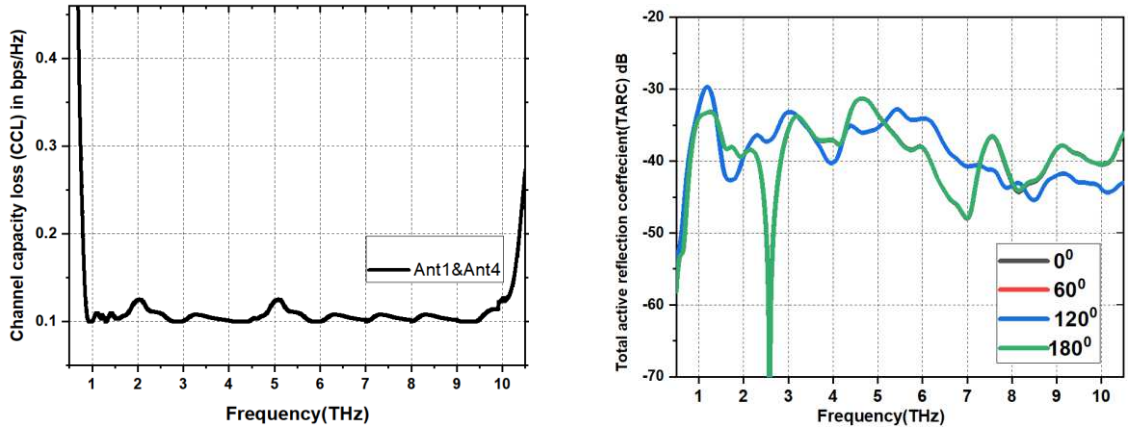

(a) (b)

Fig 13. (a)Simulated results of Channel Capacity loss (CCL) in bps/Hz (b)Simulated results of TARC (dB)

TARC is depicted as ratio of square root of total reflected power to square root of total incident power. When adjacent radiating antennas are interrupted to each other, so interruption on impedance bandwidth may affect in intended frequency spectrum. To analyse impact on impedance bandwidth, TARC computation is done by equation (16) in Saxena and Awasthi(2020).

$$TARC = \frac{\sqrt{\sum_{i=1}^{N} |b_i|^2}}{\sqrt{\sum_{i=1}^{N} |a_i|^2}} \tag{16}$$

Here a_i , b_i are amplitude of incident and reflected wave. amplitudes of incident and reflected waves are computed by scattering parameters with this “S”-matrix expression in equation (17).

$$[b] = [s][a] \tag{17}$$

Ideally total active reflective coefficient of MIMO system should be less than 0 dB in Saxena and Awasthi(2020). In Fig13(b) illustrate total active reflective coefficient(TARC)values at

phases 0^0 ,60^0 ,120^0, 180^0.TARC values are less than -30dB in intended frequency spectrum which indicates that proposed antenna is not phase-sensitive.

b. Comparison of proposed SWB MIMO antenna with Existing MIMO antennas

The characteristics of the proposed antenna are compared with most of existing SWB antennas in terms of considered parameters such as number of radiating elements, physical dimensions of antenna, impedance bandwidth, peak gain(dBi), radiation efficiency, and isolation among radiating elements. Because of the highest number of radiating elements in the proposed antenna as compared to other antennas, it exhibits the highest throughput and also resist the multipath fading in THz communication system. The radiation efficiency of proposed antenna is highest as compared to the existing antennas.

Due to its minimum physical dimensions of a single element, the proposed MIMO antenna has reduced its overall physical size and acquired highest number of radiating elements. To ensure the better performance as four port MIMO antenna, isolation among elements is high as compare to other antennas except Singhal (2020 a). Furthermore, its exhibits lower peak gain than reference antennas in Saxena and Awasthi (2020); Singhal (2020 a); and Singhal (2020 c) .However, these references are in higher profile, less radiation efficiency, or even with a smaller number of ports on larger substrate utilization is less simultaneously. Whereas value of ECC, CCL, MEG is also compared with other reported antennas. These parameter values confirm its better inter-radiating element isolation. Therefore, the proposed MIMO antenna shows superior performance than most of the THz antennas reported in literature.

Table4: Comparison of proposed work with other existing antennas

Ref. & No. of Port	**Impedance Bandwidth& % FBW**	**Gain (dBi)**	**η (%)**	**MEG (dB)**	**ECC**	**CCLb ps/Hz**	**Isolation (dB)**	**Volume(μm^3) & Dimensions in (λ)**
Singhal (2019 b) **One**	0.46-5.46THz (168%)	12	92	NR (Not required)	NR	NR	NR	800*600*81.29 polyamide 1.2 λ *0.9 λ*0.12λ
Saxena et al. (2020) **Two**	0.33-10 THz (187 %)	19	70	<-3	0.0015	0.25	<-20	1000*1400*101.3 RT5880 1.1 λ *1.54 λ *0.11 λ
Singhal (2020 a) **Two**	1.06–14.2 THz (172%)	11.2	NM	NM (Not - Measured)	<.003	0.2	<-23	820*1000* 81.29 Polyamide 2.89 λ *3.53 λ *0.29 λ
Singhal (2020 b) **Two**	0.3 - 15.1 THz(192%)	NM	NM	NM	0.02	0.2	<-13	800*1170*81.29 0.80 λ *1.17 λ *0.08 λ
Singhal (2020 c) **Two**	3.1-60THz (180%)	12	NM	NM	<.003	0.1	<-19	110*125*10 1.14 λ *1.29 λ *0.10 λ 110*155*10 1.14 λ *1.60 λ *0.10 λ
[P] **Four**	**0.9 – 10.1 THz (168%)**	**7.5**	**95**	**< -3**	**0.002**	**0.15**	**<-20**	**122.4*122.4*10 & Quartz** **0.37 λ *0.37 λ *.03 λ**

Abbreviations: P (proposed antenna), λ is the lowest frequency of operating band, η (radiation efficiency),

4. Conclusion

A SRR-CC loaded four-port MIMO antenna is proposed for super wideband (SWB) in THz intended spectrum. A planar SRR-CC structure is loaded on a semi-hexagonal patch with the partial ground to achieve the fractional bandwidth of 168% and also increase the gain at the lower frequency range for THz applications. Isolation improvement among radiating elements of the proposed MIMO antenna is achieved by applying orthogonal arrangement between radiating elements. The simulated impedance bandwidth of the proposed MIMO antenna is ranging from 0.9 to 10.1 THz with isolation of more than 20dB in the frequency spectrum. It demonstrates a stable radiation pattern with a peak gain of 7.51dBi and radiation efficiency exhibits more than 95% in the frequency spectrum. The Simulated values of performance parameters of MIMO antenna i.e. ECC, DG, MEG, TARC, CCL are in a good range for the entire frequency spectrum of operation. All simulated results indicate that the proposed MIMO antenna is a good candidate for THz applications.

References:

Muhammad Ali Jamshed, Ali Nauman, Muhammad Ali Babar Abbasi3, And Sung Won Kim," Antenna Selection and Designing for THz Applications: Suitability and Performance Evaluation: A Survey", IEEE Access PP(99):1-1 ,June 2020.

Zhang, Y.; Wang, C.; Huai,B.;Wang, S.; Zhang, Y.;Wang, D.; Rong,L.; Zheng, Y. Continuous-Wave THz Imaging for Biomedical Samples. Appl. Sci. **2021**, 11, 71. https://dx.doi.org/10.3390/app11010071

Thakur, S., & Singh, N. :Circular-slot THz antenna on PBG substrate for cancer detection. Optik, (242), 167355 (2021). .

S. Koenig, D. Lopez-Diaz, J. Antes, F. Boes, R. Henneberger, A. Leuther, A. Tessmann, R. Schmogrow, D. Hillerkuss, R. Palmer, T. Zwick, C. Koos,W. Freude, O. Ambacher, J. Leuthold, I. Kallfass, Wireless sub-THz communication system with high data rate, Nat. Photonics 7 (2013) 977–981.

Vafapour, Zohreh; Keshavarz, Afsaneh; Ghahraloud, Hossain :The potential of terahertz sensing for cancer diagnosis. Heliyon, 6(12) (2020).

Maagt P.D,: Terahertz technology for space and earth applications, International workshop on Antenna Technology: Small and Smart Antennas Metamaterials and Applications, 111–115 (2007).

Davoudabadifarahani H., and Ghalamkari B.: High efficiency miniaturized microstrip patch antenna for wideband terahertz communications applications: Optik, (194), 163118 (2019).

Kushwaha R.K., Karuppanan P., and Malviya L.: Design and analysis of novel microstrip patch antenna on photonic crystal in THz, Physica B: Condensed Matter 107–112 (2018).

Kumud R.J., Singh G.: Dual-band rectangular microstrip patch antenna at terahertz frequency for surveillance system: Journal of Computational Electronics, 31–41 (2010).

Singhal S.: Elliptical ring terahertz fractal antenna: Optik 194 163129 (2019)a.

Singhal S.: Ultrawideband elliptical microstrip antenna for terahertz applications, Microw: Opt. Technol. Lett. 61 (10) 2366–2373 (2019)b.

King C.,Station C.T.X.: Fundamentals of wireless communications.: Presented at 67th Annual Conference for Protective Relay Engineers(2014).

Varshney G.,Gotra S., Pandey V.S, Yaduvanshi R.S.: Proximity-coupled two-port multi-input-multi-output graphene antenna with pattern diversity for THz applications: Nano Communication Networks, 21 100246 1878-7789 , (2019).

Luo Y., Zeng Q., Hu X.Y.N., Xie W., Wu Y., Zhang Q.L.X.Z.: A graphene-based tunable miniaturized-element frequency selective surface in terahertz band and its application in high-isolation multiple-input multiple-output system: Micro wave and optical technology letters, 2789-2794 (2019).

Babu K.V., Das S., Varshney G., G.N.J., Madhav B.T.P.M,:A Micro-Scaled Graphene Based Tree-Shaped Wideband Printed MIMO Antenna For Terahertz Applications: Journal of Computaional Electronics.

Okan T.: High efficiency unslotted ultra-wideband microstrip antenna for sub-terahertz short range wireless communication systems: Optik, Volume 242, (2021).

Saxena G., Awasthi Y.K., Jain P.: High Isolation and High Gain Super-Wideband (0.33-10 THz) MIMO Antenna for THz Applications: Optik 223 165335 (2020).

Singhal S.: CPW Fed koch snowflake superwideband terahertz spatial diversity antenna: Optik 206 164329 (2020)a.

Singhal S.: Tetradecagonal ring shaped terahertz superwideband MIMO antenna: Optik 208 164066 (2020)b.

Singhal S.: Four arm windmill shaped superwideband terahertz MIMO fractal antenna: Optik 219 165093 (2020)c.

Davies C.L., Patel J.B., Xia C.Q., Herz L.M., Johnston M.B.: Temperature-Dependent Refractive Index of Quartz at Terahertz Frequencies: Journal of Infrared, Millimeter, and Terahertz Waves 39: 1236–1248 (2018).

Miao Z.W., Hao Z.C., Wang Y., Jin B.B., Wu J.B., and W. Hong W.: A 400-GHz high-gain quartz-based single layered folded rectarray antenna for terahertz applications: *IEEE Trans. Terahertz Sci. Technol.*, vol. 9,no.1,pp.78_88,Jan.(2019).

Thummaluru S.R., Ameen M., Chaudhary R.K.: Four-port MIMO cognitive radio system for midband 5G applications: IEEE Transactions on Antennas and Propagation 67 (8), 5634-5645,May.(2019).

Tung N., Lam V., Park J., Cho M., Rhee J., Jang W.: Single-and double-negative refractive indices of combined metamaterial structure: J Appl Phys, 106 053109 (2009).

Ali W.A., Mohamed H.A., Ibrahim A.A., Hamdalla M.Z.: Gain improvement of tunable band-notched UWB antenna using metamaterial lens for highspeed wireless communications: Microsyst. Technol. 25 4111–4117(2019).

He X., Qiu J., Wang L.Y., Geng Z.X., Wang J.M., Gui T.L.: A compact thin-film sensor based on nested split-ring-resonator (SRR) metamaterials for microwave applications: J Infrared Millimeter Terahertz Waves.;32:902–913 (2011).

Smith D.R, Schultz S., Markoš P., Soukoulis C.: Determination of effective permittivity and permeability of metamaterials from reflection and transmission coefficients: Phys Rev B;65 195104 (2002).

Cao W., Singh R., Naib I.A., He M., Taylor A.J., Zhang W.: Low-loss ultra-high-Q dark mode plasmonic Fano metamaterials: Opt Lett. 3366–3368, Aug. (2012).

Iqbal A., Saraereh O. A, Bouazizi A., and Basir A.: Metamaterial-based highly isolated MIMO antenna for portable wireless applications: *Electronics*, vol. 7, no. 10, p. 267, Oct. (2018).

Iqbal A., Bouazizi A., Kundu S., Elfergani I., and Rodriguez J.: Dielectric resonator antenna with top loaded parasitic strip elements for dual-band operation: *Microw. Opt. Technol. Lett.*, vol. 61, no. 9, pp. 2134_2140, Sep. (2019).

Pan, B. C.: Reduction of the spatially mutual coupling between dual-polarized patch antennas using coupled metamaterial slabs.: Sci. Rep. 6, 30288, (2016).

Balmaz P.G., Martin O.J.F.: Electromagnetic resonances in individual and coupled split-ring resonators: J Appl Phys ;92:2929–36 (2002).